Laser ablation-inductively coupled plasma-mass spectrometry imaging of white and grey matter iron distribution in Alzheimer's disease frontal cortex

Dominic J. Hare[ab†], Erika P. Raven[cd†], Blaine R. Roberts[b], Mirjana Bogeski[b], Stuart D. Portbury[b], Catriona A. McLean[ef], Colin L. Masters[b], James R. Connor[gh], Ashley I. Bush[b], Peter J. Crouch[i], and Philip A. Doble[a**]*

[a] *Elemental Bio-imaging Facility, University of Technology Sydney, Australia.*
[b] *The Florey Institute of Neuroscience and Mental Health, The University of Melbourne, Australia.*
[c] *Center for Functional and Molecular Imaging, Georgetown University Medical Center, United States of America*
[d] *Advanced Magnetic Resonance Imaging Section, Laboratory of Functional and Molecular Imaging, National Institute of Neurological Disorders and Stroke, National Institutes of Health, United States of America*
[e] *Department of Anatomical Pathology, Alfred Hospital, Australia*
[f] *Department of Medicine, Central Clinical School, Monash University, Australia*
[g] *Department of Neural and Behavioral Sciences, Penn State Hershey Medical Center, United States of America*
[h] *Department of Neurosurgery, Penn State Hershey Medical Center, United States of America*
[i] *Department of Pathology, School of Biomedical Sciences, University of Melbourne, Australia*

* *Correspondence to: Dominic J. Hare, University of Technology Sydney, PO Box 123, Broadway, New South Wales, 2007, Australia. Email. dominic.hare@uts.edu.au; Ph. +61 3 9035 9549*
** *Correspondence to: Philip A. Doble, University of Technology Sydney, PO Box 123, Broadway, New South Wales, 2007, Australia. Email. philip.doble@uts.edu.au; Ph. +61 2 9514 1792*

[†] *These authors contributed equally.*

Abstract

Iron deposition in the brain is a feature of normal aging, though in several neurodegenerative disorders, including Alzheimer's disease, the rate of iron accumulation is more advanced than in age-matched controls. Using laser ablation-inductively coupled plasma-mass spectrometry imaging we present here a pilot study that quantitatively assessed the iron content of white and grey matter in the frontal cortex of Alzheimer's and control subjects. Using the phosphorus image as a confirmed proxy for the white/grey matter boundary, we found that intrusion of iron into grey matter occurs in the Alzheimer's brain compared to controls, which may be indicative of either a loss of iron homeostasis in this vulnerable brain region, or provide evidence of increased inflammatory processes as a response to chronic neurodegeneration. We also observed a trend of increasing iron within the white matter of the frontal cortex, potentially indicative of disrupted iron metabolism preceding loss of myelin integrity. Considering the known potential toxicity of excessive iron in the brain, our results provide supporting evidence for the continuous development of novel magnetic resonance imaging approaches for assessing white and grey matter iron accumulation in Alzheimer's disease.

Introduction

Increased iron deposition in the cerebral cortex of Alzheimer's disease (AD) brains is a pathological hallmark of the condition (Hallgren and Sourander, 1960). Neuroinflammation, where glial cells promote the deposition of iron, contributes to elevated oxidative stress and mitochondrial dysfunction, and may also promote the aggregation of the β-amyloid peptide and tau protein, forming the plaques and tangles characteristic of the disease (Ong and Farooqui, 2005). Combined with the natural accumulation of iron in the aging brain, endogenous response to elevated cortical iron (such as heme oxygenase-1, which degrades heme and can release free, reactive ferrous [Fe^{2+}] iron) may represent an important biochemical mechanism preceding neuronal damage in AD (Ward et al., 2014).

In vivo imaging of the AD brain using magnetic resonance imaging (MRI) has provided useful insight into both structural changes (Bartzokis et al., 2003) and iron deposition (Bartzokis et al., 2000; Langkammer et al., 2014), using techniques such as R_2 and R_2* relaxometery (Langkammer et al., 2010), phase imaging (Zhu et al., 2009) and quantitative susceptibility mapping (Bilgic et al., 2012). However, differentiation between white and grey matter iron distribution in the neocortex using MRI is challenging, as typical MRI approaches are not absolutely quantitative, there are multiple contributions to tissue contrast (including myelin, iron and CSF), and have a spatial resolution that precludes fine detail definition of brain iron distribution at micrometer scales. Because of these many limitations, MR imaging of brain iron has been largely constrained to deep brain nuclei, such as the basal ganglia, which contain the highest iron content throughout the brain.

In this study we employed quantitative iron imaging by laser ablation-inductively coupled plasma-mass spectrometry (LA-ICP-MS) to compare the distribution of iron in white and grey matter regions of *post mortem* AD and healthy control (HC) frontal cortex tissue which are primarily affected by AD pathology. LA-ICP-MS employs a focused beam (typically in the ultra-violet range) that ablates particles from the tissue sample surface, which are then carried to the ICP-MS and measured on the basis of mass-to-charge (*m/z*) ratio (Hare et al., 2015). LA-ICP-MS is highly specific and sensitive to iron, with detection limits well below the typical biological concentrations

found in neurological tissue (O'Reilly et al., 2014). With appropriate signal normalization and periodic sampling of standards with comparable matrix composition, LA-ICP-MS can provide absolute quantitative information at the low micrometer scale (1-100+ µm) (Hare et al., 2012a; Miliszkiewicz et al., 2015). As an element-specific detector, LA-ICP-MS also permits simultaneous detection of multiple analytes and generation of hyperspectral images. We exploited this capability here by using phosphorus distribution as a proxy for white and grey matter, which was then applied to differentiating iron distribution in the two regions of frontal cortex tissue from both AD and HC brains.

Materials and methods:

Human brain samples

Formalin fixed and paraffin embedded AD (n = 4) and HC (n = 5) frontal cortex tissue was obtained from the Victorian Brain Bank Network at the Florey Institute of Neuroscience and Mental Health. All procedures were conducted in accordance with the Australian National Health and Medical Research Council's National Statement on Ethical Conduct in Human Research (2007), the Victorian Human Tissue Act (1982), the National Code of Ethical Autopsy Practice (2002) and the Victorian Government policies and practices in relation to *post mortem* tissue. All tissue samples were previously genotyped and confirmed as apolipoprotein E3/E3 allele carriers (Rembach et al., 2013). Subject details are given in Tables 1 and 2. Previous studies have shown that formalin fixation may effect absolute iron concentrations (Hackett et al., 2011; Hare et al., 2014a), particularly during long-term (approx. 4 years) storage of brain tissue (Schrag et al., 2010). However, storage in formalin for shorter periods (<18 months) was shown to have no effect on brain iron levels (Gellein et al., 2007). Regardless, all samples underwent identical preparation methods (fixation of whole brain in 20% neutral buffered formalin for <6 weeks prior to neuropathological examination, excision of tissue blocks, paraffin infiltration and embedding) to ensure relative comparisons were valid.

Table 1: Subject age, sex and *post mortem* interval details. Neither age ($p = 0.2$; Student's two-tailed *t*-test) nor *post mortem* interval ($p = 0.3$) differed between groups.

	Alzheimer's disease	**Healthy control**
Age (years)	74.2 ± 8.0 ($n = 4$)	85.4 ± 2.1 ($n = 5$)
Male (female)	4 (0)	4 (1)
Post mortem interval (hours)	47.9 ± 11.9	34.5 ± 5.7

Table 2: Disease duration, cause of death and AD family history (where applicable).

Case	**Disease duration**	**Cause of death**	**Family history**
AD1	~ 4 years, 6 months (early onset at ~ 49 years)	Pulmonary thromboembolism; deep vein thrombosis	Mother AD onset in her 70s, grandmother also had AD
AD2	~ 4 years	Dementia	Not known
AD3	Unsure (never saw regular doctor); minimum 4 yrs	Acute septicaemia; dementia	Mother AD onset in her late 80s
AD4	Diagnosed 18 months prior to death, date of onset not known	Multiple myeloma; cerebral arteriosclerosis	No family history
HC1	n/a	Cardiac tamponade – haemopericardium, ruptured acute posterolateral left; ventricular myocardial infarction; ischaemic coronary artery disease	
HC2	n/a	Acute myocardial infarction; ischaemic heart disease; hypertension	
HC3	n/a	Acute myocardial infarction	
HC4	n/a	Complications of surgical correction of fractured neck of femur; general debility; hepatic abscess; ischaemic heart disease; chronic renal failure	
HC5	n/a	Ischaemic Heart Disease	

Sample preparation for LA-ICP-MS

Sections were cut on a standard microtome at 5-µm thickness and mounted on silane-coated soda-glass microscope slides (StarFrost®; ProSciTech, Qld, Australia). Sections were dewaxed in xylene (Merk Millipore, NSW, Australia) and decreasing concentrations of ethanol (Merk Millipore) in water according to standard protocols. Samples were finally washed in MilliQ water (18.2 MΩ; Merk Millipore) and dried at room temperature before analysis.

LA-ICP-MS analysis

Quantitative imaging of iron was performed using a NewWave NWR213 laser ablation system (ESI Ltd., Bozeman, MT, USA) hyphenated to an Agilent Technologies 8800 Series triple quadrupole ICP-MS (Mulgrave, VIC, Australia) operating in single quadrupole acquisition mode with 3 mL min^{-1} hydrogen reaction gas to minimize polyatomic interference from $^{40}Ar^{16}O^{+}$ on $^{56}Fe^{+}$ (Lear et al., 2012). The NWR213 was fitted with a standard two-volume cell with a 10 cm x 10 cm scanning area. Standard operating parameters for this system were used as previously reported (Bishop et al., 2015). Mass-to-charge (*m/z*) ratios for carbon (13), phosphorus (31) and iron (56) were acquired. Samples were ablated using a square 80 x 80 µm laser beam, producing pixels representing a total area of 6.4 mm^2 with a laser energy fluence of approximately 1 J cm^{-2}, which was sufficient to ablate tissue but not the underlying slide matrix. Signal noise accounted for approximately 0.3% of the mean signal intensity for each section, and was thus considered negligible. Phosphorus and iron data was normalized to the corresponding carbon-13 signal recorded to compensate for variation in laser power and sample transport effects (Austin et al., 2011). Iron images were quantitated against representative ablation (carbon-13 normalized) of matrix-matched tissue standards produced using metal-spiked homogenates of sheep cortical brain tissue cut to an equivalent thickness on a cryostat (Hare et al., 2013b). Four repeated five-point calibrations were recorded during the experiment, with good linearity (r^2 = 0.9485) and reproducibility (p = 0.4677; F = 0.909; Supplementary Fig. S1). Images were produced using ENVI 5.3 (Exelis, Boulder, CO, USA), background (scanned areas not containing tissue) pixels excluded using a carbon-13 mask, and regions of interest (ROIs) were extracted using both ENVI 5.3 and Fiji (http://fiji.sc/Fiji, (Schindelin et al., 2012)). Statistical analysis of extracted ROIs was performed using Prism 6.0e (GraphPad, La Jolla, CA, USA)

Perls staining

Adjacent 5-µm thick sections mounted on microscope slides were dewaxed as above, and then extensively rinsed in running water. Hydrated sections were incubated at 37 °C for 1 hour in potassium ferrocyanide (7% w/v) in hydrochloric acid (3% v/v) and then enhanced using a solution of 3.5 µM 3,3'-diaminobenzidine (DAB) in hydrogen peroxide (0.015% v/v) for 5 minutes. After quenching the reaction by immersing in running water, samples were counterstained with hemotoxylin for 2 minutes and

washed in water before dehydration in increasing ethanol concentration, xylene and coverslipping. Micrographs were recorded using a Leica DM2500 optical microscope with a 2.5×/0.50 NA lens and Leica DFC310FX digital camera.

Myelin staining

Myelin was histologically stained on additional adjacent 5-µm thick sections using the Luxol Fast Blue method. Sections were dewaxed and stained in 0.1% (w/v) Luxol Fast Blue in methanol with 0.05% (v/v) acetic acid for 1 hour. White and grey matter was differentiated in 0.05% (w/v) lithium carbonate for approximately 4 minutes. Sections were then counterstained with Cresyl Violet for 1 hour, dehydrated, cleared in xylene and coverslipped. Micrographs were recorded the same equipment as described above.

Results:

Quantitative images of iron in the AD and HC sections are presented in Fig. 1a (shown here on the same scale, see Supplementary Fig. S2 for individually scaled images). In AD tissue, total iron was elevated compared to control (mean iron concentration AD = 18.80 ± 2.23 µg g^{-1}; HC = 12.80 ± 1.17 µg g^{-1}; $p < 0.05$, Student's two-tailed *t*-test; Fig. 1b). Perls staining with DAB enhancement (Fig. 1a) revealed only minor non-heme iron deposition within white matter. Iron could be associated with three specific distribution patterns in both AD and HC tissue in each LA-ICP-MS image related to both grey and white matter myelin content: i) cortical 'bands' of tangentially oriented, myelinated fiber tracts (*e.g.* Bands of Baillarger), consistent with layer-specific MR contrast variations attributed to the co-localization of these myelin bands with iron (Fukunaga et al., 2010); ii) subcortical U-fibers found directly adjacent to the white-grey matter boundary (Drayer et al., 1986); and iii) non-homogenous pattern in subcortical white matter in the form of a diffuse, patchwork distribution previously reported using immunohistochemistry by Connor and Menzies (Connor and Menzies, 1995) and in subsequent mouse studies using LA-ICP-MS (Hare et al., 2014b).

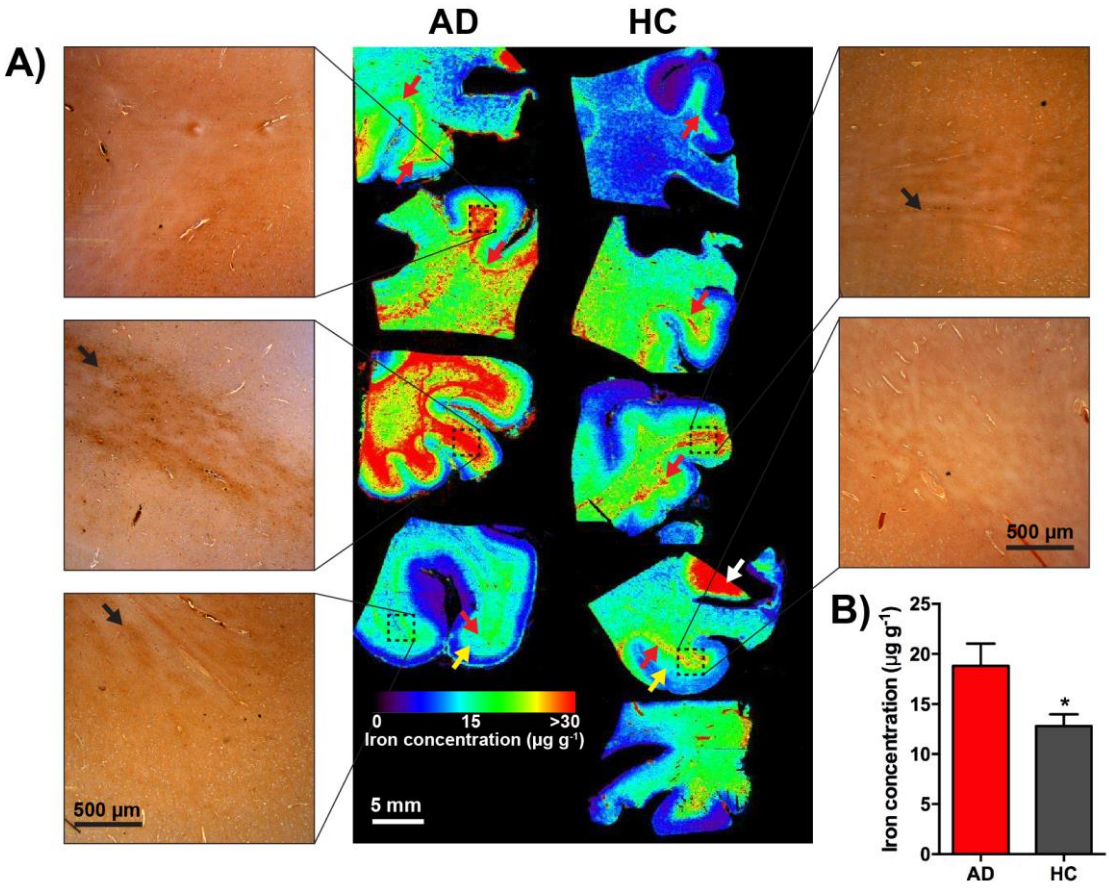

Fig. 1. A) Quantitative LA-ICP-MS imaging of total iron levels in AD and HC frontal cortex sections and corresponding Perls images from selected regions of interest. Perls staining with DAB enhancement revealed only minor intracellular increases in iron content visible within the white matter of AD brains, mirroring the 'streaking' pattern within these regions observed in LA-ICP-MS images, which was less obvious in age-matched HCs. Red arrows indicate subcortical iron, yellow arrows indicate cortical iron (see Supplementary Fig. S2). B) The total frontal cortex iron levels were significantly increased (*; $p < 0.05$; Student's two-tailed *t*-test) in the AD sections. Error bars = 1 standard deviation between samples. Note: the white arrow indicates iron-rich caudate nucleus in one section, which was confirmed by Luxol Fast Blue staining and was excluded from the analysis.

To demarcate the white-grey matter boundary, we used images of phosphorus (Fig. 2a; Supplementary Fig. S3), which has been shown to effectively depict spatial myelin distribution using micro particle induced X-ray emission spectroscopy (µPIXE) with myelin immunostaining as a confirmatory comparator (Stüber et al., 2014), and is more concentrated in white matter (Duyn et al., 2007). LA-ICP-MS imaging is hyperspectral, where iron and phosphorus signal corresponds between pixels. A white matter mask was produced by a threshold function using bimodal distribution of phosphorus pixels. A grey matter mask was then produced using the remaining pixels with the white matter values excluded. This mask was then applied

to iron images (Fig. 3). We confirmed that phosphorus imaging by LA-ICP-MS also delineated white and grey matter with Luxol Fast Blue staining of myelin (Fig. 2a). There was no apparent difference in relative phosphorus distribution between AD and HC groups (WM_{AD} = 2.53 ± 0.24, WM_{HC} = 2.53 ± 0.05, p = 1.0; GM_{AD} = 1.50 ± 0.14, GM_{HC} = 1.55 ± 0.06; p = 0.7; all units carbon-13 normalized phosphorus signal intensity; Supplementary Fig. S4). Iron was present at a lower concentration in grey matter of the HC frontal cortex (WM_{HC} = 15.1 ± 1.7 µg g^{-1}; GM_{HC} = 10.5 ± 1.1 µg g^{-1}; $p < 0.05$; iron concentrations for each section are shown in Table 2), though in corresponding AD sections the demarcation of iron distribution within white and grey matter was lost (WM_{AD} = 18.7 ± 3.7 µg g^{-1}; GM_{AD} = 15.7 ± 2.2 µg g^{-1}; p = 0.7). Comparing white and grey matter between AD and HC tissue, we found that iron was significantly elevated in the grey matter of AD brains (+49%; $p < 0.05$), and showed a generalized, non-significant increasing trend in white matter (+25%; p = 0.4; Fig. 2b). It is unclear as to why errors associated with iron in AD tissue were generally larger than HC samples, though we have observed that cellular iron dyshomeostasis, such as is thought to be involved in AD pathology, demonstrates a more variable concentration of iron, indicative of a system in crisis (James et al., 2016).

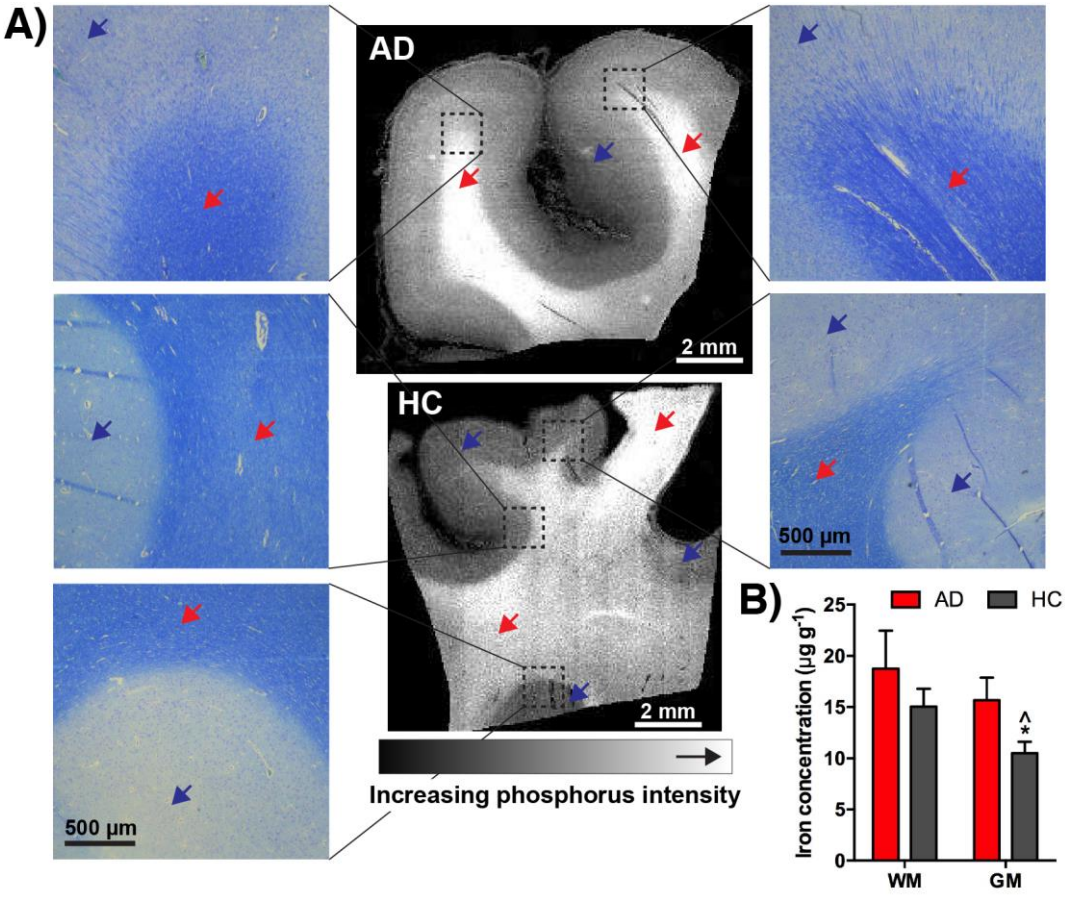

Fig. 2. A) Myelin staining using the Luxol Fast Blue method confirms phosphorus imaging by LA-ICP-MS differentiates white (red arrows) and grey matter (blue arrows). B) Using the phosphorus images to delineate the white/grey matter boundary and simultaneously obtained iron LA-ICP-MS images, iron levels were quantified according to white/grey matter distribution. Iron levels in white matter did not differ significantly between experimental groups, though iron was significantly increased in the grey matter of the AD frontal cortex (*; $p < 0.05$; Student's two-tailed *t*-test). Also, the significant difference between white and grey matter in healthy controls (^; $p < 0.05$) was not observed in AD tissue sections ($p = 0.5$).

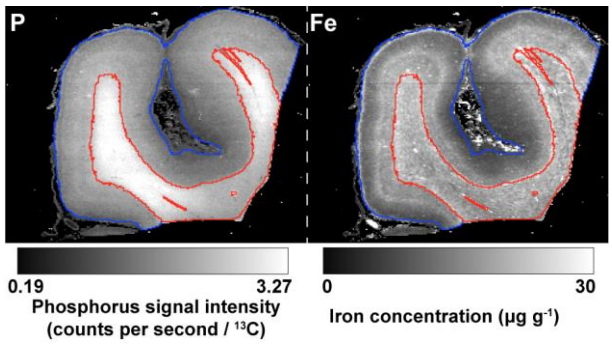

Fig. 3: Masks were generated using high (white matter; red line) and low phosphorus signal intensity values, which were then applied to quantitative iron images to extract white and grey matter regions of interest.

Table 3: Individual iron concentrations (± 1 standard deviation) and total measured area in whole brain, white matter and grey matter for AD and HC sections analysed.

	Whole brain		**White matter**		**Grey matter**	
Case	Iron (μg g^{-1})	Area (mm^2)	Iron (μg g^{-1})	Area (mm^2)	Iron (μg g^{-1})	Area (mm^2)
AD1	15.0 ± 13.2	150.2	13.8 ± 5.2	44.3	15.6 ± 7.2	105.9
AD2	19.1 ± 12.1	171.2	19.5 ± 4.7	69.3	17.1 ± 6.3	101.9
AD3	23.5 ± 18.9	168.5	28.9 ± 10.8	94.2	20.2 ± 8.7	74.3
AD4	10.6 ± 4.4	188.4	12.8 ± 2.8	129.8	9.8 ± 3.6	58.6
HC1	8.4 ± 4.9	180.1	9.0 ± 3.0	55.2	7.2 ± 4.1	124.9
HC2	15.3 ± 6.8	155.7	16.4 ± 4.8	41.6	13.4 ± 7.9	114.1
HC3	13.8 ± 7.0	173.3	19.5 ± 5.1	130.3	12.0 ± 5.0	43.0
HC4	13.0 ± 4.1	146.1	14.3 ± 3.8	67.8	11.0 ± 4.0	78.2
HC5	13.3 ± 10.3	148.3	16.1 ± 9.3	61.6	9.0 ± 10.0	86.7

Discussion

Previously reported iron levels in digests of formalin-fixed frontal white matter, measured using solution nebulization ICP-MS, were markedly higher than our results; iron concentrations were ~50% of those reported in fixed frontal lobe tissue reported by others (Langkammer et al., 2012a; Langkammer et al., 2012b). However, leaching did not appear to be specific to cortical tissue; the iron concentration in the caudate nucleus excluded from our analysis (33.0 ± 10.9 μg g^{-1}) showed a similar degree of iron loss compared to non-embedded tissue (Langkammer et al., 2012b). To our knowledge, the effects of paraffin embedding and deparaffinization on brain iron levels has not been reported, though a study comparing fresh liver tissue to paraffin infiltrated and dewaxed samples showed a linear relationship between iron concentrations *in lieu* of absolute quantitative reproducibility (Beilby et al., 1999). Regardless, and as stated in the Methods and Materials, all samples underwent identical preparation steps to ensure valid comparisons. While it is possible that an altered chemical environment with respect to iron in AD tissue is more susceptible to *post mortem* artefact, such as leaching during the fixation and embedding process, the hypothesis that neurotoxicity in AD is related to an increased labile iron pool (*i.e.* Fe^{2+}) (Peters et al., 2015) is supported by our data, which shows elevated iron levels are preserved in AD tissue even after extensive chemical treatment. However, speciation of iron is not practical for archived tissue sections nor this analytical approach; fresh unfixed tissue and species-specific imaging such as X-ray absorption

near-edge structure (XANES) spectroscopy would be required for this task (James et al., 2016).

Although subcortical white matter contains some of the lowest concentration of iron within the brain (Riederer et al., 1989), particularly compared to the basal ganglia (Hare et al., 2012b)., and corresponding cortical grey matter also contains comparatively less non-heme iron (Hallgren and Sourander, 1960). Our results from age-matched healthy controls show that cortical grey matter contains less *total* iron than adjacent white matter. These data are in agreement with historical values; Hallgren and Sourander (1958) reported that the ratio of iron in frontal white matter to temporal cortex was 1.3, and we observed a similar ratio of 1.5.

Our results highlight some of the known limitations of MRI for assessing brain iron levels. Myelin is known to introduce significant bias in magnetic susceptibility MRI (Lodygensky et al., 2012), with this bias strongest in myelin-rich white matter. Field dependent relaxation rate increase (FDRI) MRI is more robust to ferritin iron content, although is susceptible to registration error between scanning sessions (Daugherty and Raz, 2015). Thus, *in vivo* assessment of iron accumulation is often most suited to diseases affecting areas of natively high iron and low myelin content, such as the basal ganglia in Parkinson's disease (Rossi et al., 2013).

This is not to say that iron concentration in the cerebral white matter does not play a significant role in brain aging and age-related disorders like AD. Numerous histological and MRI studies have identified significant age-related changes first appearing in the cerebral white matter (Gunning-Dixon et al., 2009). R_1 with diffusion MRI of white matter measured over a large cohort spanning 80 years identified a slow decline beginning at 40+ years of age (Yeatman et al., 2014). Central to the brain iron deposition and free radical theory of aging is that a loss of iron homeostasis results in the accumulation of reactive iron(II), which mediates the generation of harmful reactive oxygen species (ROS) (Schipper, 2004). This occurrence may not necessarily result in a measure of accumulation of iron. Rather, the redistribution of iron from safe storage in proteins like ferritin to the cytoplasm may be sufficient to initiate a cascading Fenton reaction, where iron repeatedly cycles through the ferrous and ferric oxidation states to produce a constant source of free radicals that eventually

overwhelm endogenous antioxidant mechanisms (Hare et al., 2013a). Therefore, lower iron levels in white matter compared to the deep brain structures of the basal ganglia should not be viewed as an insignificant contributor to either normal brain aging, or age-related neurodegeneration, such as AD. White matter is particularly lipid-rich, and thus highly susceptible to peroxidation and loss of cellular and structural integrity in AD (Bartzokis et al., 2003).

The generalized increase in cortical grey matter iron in our pilot study lends further support to iron playing a critical role in neurodegeneration within the AD brain. Disrupted iron metabolism, such as impaired activity of the amyloid precursor protein (Duce et al., 2010), which is essential to the stabilization of the membrane-bound iron export protein ferroportin (Wong et al., 2014), can lead to an increase in the labile iron pool within neurons, facilitating increased ROS generation. When combined with R_2 relaxometry, FDRI MRI has shown a relationship between iron accumulation in ferritin and loss of tissue integrity in the hippocampus of AD patients (Raven et al., 2013). Iron has also been associated with accumulation around extracellular amyloid plaques in humans (Connor et al., 1992a; Lovell et al., 1998). Our LA-ICP-MS technique likely lacks the resolution to discern these microscopic structures (Lovell et al.'s study used micro-particle induced X-ray emission spectroscopy with a per-pixel resolution of 50 μm^2), though a study using X-ray fluorescence microscopy with a similar resolving power (60 μm^2) found elevated extracellular iron in the PSAPP mouse model of AD that displays similar plaque pathology was *not* associated with the β-amyloid inclusions (Leskovjan et al., 2011).

Intrusion of iron into the grey matter of AD frontal cortex supports MRI studies that have identified a loss in grey matter density (used as a proxy for atrophy) that correlates with cognitive decline (Frisoni et al., 2002) and occurs at an increased rate in AD (Thompson et al., 2003). Increased iron in the grey matter may indicate either a loss of iron homeostasis, or a brain region at higher risk of iron-mediated neurodegeneration. Previous studies of iron regulatory proteins in cortical tissue found a generalized decrease in transferrin levels in grey matter and consistent distribution of ferritin (Connor et al., 1992b). This may be indicative a higher degree of ferritin saturation as a compensatory mechanism for increased grey matter iron, though Perls staining did not reveal an observable amount of increased non-heme iron

within this region. Another possible scenario reflective of increased grey matter iron is the inflammatory process underway within the degenerating region. *In vitro* studies of astrocytes and microglia cultured from *post mortem* AD white and grey matter has shown grey matter-sourced cells proliferate more rapidly than white matter counterparts (Blasko et al., 2004). Our hypothesis is supported by a recent study using high field 7 Tesla MRI and histological assessment (*via* the same Perls-DAB method employed here) of *post mortem* AD tissue, which showed correlation between grey matter iron and activated microglia in AD, as well as a similar staining within white matter (Zeineh et al., 2015). This pattern of non-heme iron is consistent with elevated levels of ferritin within white matter (Fukunaga et al., 2010; van Duijn et al., 2013), and the more prominent Perls staining in AD tissue may also be reflective of the pathological accumulation of this iron storage protein previously observed in the hippocampus (Raven et al., 2013), preceding a loss of structural integrity in the frontal cortex white matter occurring later in the disease. Chronic inflammation is a cardinal feature of AD (Gomez-Nicola and Boche, 2015) and neurodegeneration in general (De Lucia et al., 2015), and targeting inflammatory pathways and microglial activation is a promising avenue for therapeutic development (Olmos-Alonso et al., 2016). Our observed increase in iron levels within the degenerating grey matter supports that this region is under duress and initiates a response mechanism highly dependent on iron-mediated enzymatic processes, which in turn has a follow-on effect on oligodendrocyte health and myelin integrity in white matter. Further, hypometabolism (which is associated with iron deposition and white matter damage in the aceruloplasmenic brain (Miyajima et al., 2002)) occurs prior to atrophy in AD white matter (Chételat et al., 2008), with the frontal cortex displaying loss of integrity comparatively later in the disease than more posterior regions (Medina et al., 2006).

Conclusions

We have demonstrated that *post mortem* analysis of frontal cortex tissue from AD and HC subjects displays a marked change in cortical grey matter iron distribution in this degenerating region of the brain. Although this method is only possible using *post mortem* tissue, we present important supporting evidence for existing MRI studies that have focused on discerning white and grey matter iron distributions *in vivo* using a highly sensitive and quantitative imaging approach. Results from this study highlight

a further need to understand the mechanisms by which iron may impart neurotoxicity in AD.

Acknowledgements

The authors would like to thank Dr Ian Birchall and Dr Jeff Duyn for their helpful advice, and Ms Fairlie Hilton of the Victorian Brain Bank Network for her assistance. D.J.H. and P.A.D. are supported by funds from Australian Research Council Linkage Project (LP120200081) in conjunction with ESI Ltd and Agilent Technologies. D.J.H. and B.R.R. are additionally supported through Australian Research Council Linkage Project (LP140100095) with Agilent Technologies. E.P.R. is supported by the National Science Foundation Graduate Research Fellowship under Grant No. DGE-1444316. P.J.C. is supported by funds from the National Health and Medical Research Council (1005651 and 1061550). We gratefully acknowledge the support of the Victorian Government's Operational Infrastructure Support Program and the Victorian Brain Bank Network.

References:

Austin, C., Fryer, F., Lear, J., Bishop, D., Hare, D.J., Rawling, T., Doble, P., 2011. Factors affecting internal standard selection for quantitative elemental bio-imaging of soft tissues by LA-ICP-MS. Journal of Analytical Atomic Spectrometry 26, 1494-1501.

Bartzokis, G., Cummings, J.L., Sultzer, D., Henderson, V.W., Nuechterlein, K.H., Mintz, J., 2003. White Matter Structural Integrity in Healthy Aging Adults and Patients With Alzheimer Disease: A Magnetic Resonance Imaging Study. Archives of Neurology 60, 393-398.

Bartzokis, G., Sultzer, D., Cummings, J., Holt, L.E., Hance, D.B., Henderson, V.W., Mintz, J., 2000. In vivo evaluation of brain iron in Alzheimer disease using magnetic resonance imaging. Archives of General Psychiatry 57, 47-53.

Beilby, J.P., Prins, A.W., Swanson, N.R., 1999. Determination of hepatic iron concentration in fresh and paraffin-embedded tissue. Clinical Chemistry 45, 573-574.

Bilgic, B., Pfefferbaum, A., Rohlfing, T., Sullivan, E.V., Adalsteinsson, E., 2012. MRI estimates of brain iron concentration in normal aging using quantitative susceptibility mapping. NeuroImage 59, 2625-2635.

Bishop, D.P., Clases, D., Fryer, F., Williams, E., Wilkins, S., Hare, D.J., Cole, N., Karst, U., Doble, P.A., 2015. Elemental bio-imaging using laser ablation-triple quadrupole-ICP-MS. Journal of Analytical Atomic Spectrometry.

Blasko, I., Stampfer Kountchev, M., Robatscher, P., Veerhuis, R., Eikelenboom, P., Grubeck Loebenstein, B., 2004. How chronic inflammation can affect the brain and support the development of Alzheimer's disease in old age: the role of microglia and astrocytes. Aging Cell 3, 169-176.

Chételat, G., Desgranges, B., Landeau, B., Mézenge, F., Poline, J.B., de la Sayette, V., Viader, F., Eustache, F., Baron, J.C., 2008. Direct voxel-based comparison between grey matter hypometabolism and atrophy in Alzheimer's disease. Brain 131, 60-71.

Connor, J.R., Menzies, S.L., 1995. Cellular management of iron in the brain. Journal of the Neurological Sciences 134 Suppl, 33-44.

Connor, J.R., Menzies, S.L., St Martin, S.M., Mufson, E.J., 1992a. A histochemical study of iron, transferrin, and ferritin in Alzheimer's diseased brains. Journal of Neuroscience Research 31, 75-83.

Connor, J.R., Snyder, B.S., Beard, J.L., Fine, R.E., Mufson, E.J., 1992b. Regional distribution of iron and iron-regulatory proteins in the brain in aging and Alzheimer's disease. Journal of Neuroscience Research 31, 327-335.

Daugherty, A.M., Raz, N., 2015. Appraising the Role of Iron in Brain Aging and Cognition: Promises and Limitations of MRI Methods. Neuropsychology Review 25, 272-287.

De Lucia, C., Rinchon, A., Olmos-Alonso, A., Riecken, K., Fehse, B., Boche, D., Perry, V.H., Gomez-Nicola, D., 2015. Microglia regulate hippocampal neurogenesis during chronic neurodegeneration. Brain, Behavior, and Immunity. DOI:10.1016/j.bbi.2015.11.001

Drayer, B., Burger, P., Darwin, R., Riederer, S., Herfkens, R., Johnson, G.A., 1986. MRI of brain iron. American Journal of Roentgenology 147, 103-110.

Duce, J.A., Tsatsanis, A., Cater, M.A., James, S.A., Robb, E., Wikhe, K., Leong, S.L., Perez, K., Johanssen, T., Greenough, M.A., Cho, H.-H., Galatis, D., Moir, R.D., Masters, C.L., McLean, C., Tanzi, R.E., Cappai, R., Barnham, K.J., Ciccotosto, G.D., Rogers, J.T., Bush, A.I., 2010. Iron-Export Ferroxidase Activity of β-Amyloid Precursor Protein Is Inhibited by Zinc in Alzheimer's Disease. Cell 142, 857-867.

Duyn, J.H., van Gelderen, P., Li, T.-Q., de Zwart, J.A., Koretsky, A.P., Fukunaga, M., 2007. High-field MRI of brain cortical substructure based on signal phase. Proceedings of the National Academy of Sciences of the United States of America 104, 11796-11801.

Frisoni, G., Testa, C., Zorzan, A., Sabattoli, F., Beltramello, A., Soininen, H., Laakso, M., 2002. Detection of grey matter loss in mild Alzheimer's disease with voxel based morphometry. Journal of Neurology, Neurosurgery and Psychiatry 73, 657-664.

Fukunaga, M., Li, T.-Q., van Gelderen, P., de Zwart, J.A., Shmueli, K., Yao, B., Lee, J., Maric, D., Aronova, M.A., Zhang, G., Leapman, R.D., Schenck, J.F., Merkle, H., Duyn, J.H., 2010. Layer-specific variation of iron content in cerebral cortex as a source of MRI contrast. Proceedings of the National Academy of Sciences of the United States of America 107, 3834-3839.

Gellein, K., Flaten, T.P., Erikson, K.M., Aschner, M., Syversen, T., 2007. Leaching of Trace Elements from Biological Tissue by Formalin Fixation. Biological Trace Element Research 121, 221-225.

Gomez-Nicola, D., Boche, D., 2015. Post-mortem analysis of neuroinflammatory changes in human Alzheimer’s disease. Alzheimer's Research and Therapy 7, 1.

Gunning-Dixon, F.M., Brickman, A.M., Cheng, J.C., Alexopoulos, G.S., 2009. Aging of Cerebral White Matter: A Review of MRI Findings. International Journal of Geriatric Psychiatry 24, 109-117.

Hackett, M.J., McQuillan, J.A., El-Assaad, F., Aitken, J.B., Levina, A., Cohen, D.D., Siegele, R., Carter, E.A., Grau, G.E., Hunt, N.H., Lay, P.A., 2011. Chemical alterations to murine brain tissue induced by formalin fixation: implications for biospectroscopic imaging and mapping studies of disease pathogenesis. The Analyst 136, 2941.

Hallgren, B., Sourander, P., 1958. The effect of age on the non-haemin iron in the human brain. Journal of Neurochemistry 3, 41-51.

Hallgren, B., Sourander, P., 1960. The non-haemin iron in the cerebral cortex in Alzheimer's disease. Journal of Neurochemistry 5, 307-310.

Hare, D.J., Austin, C., Doble, P., 2012a. Quantification strategies for elemental imaging of biological samples using laser ablation-inductively coupled plasma-mass spectrometry. The Analyst 137, 1527-1537.

Hare, D.J., Ayton, S., Bush, A., Lei, P., 2013a. A delicate balance: Iron metabolism and diseases of the brain. Frontiers in Aging Neuroscience 5.

Hare, D.J., George, J.L., Bray, L., Volitakis, I., Vais, A., Ryan, T.M., Cherny, R.A., Bush, A.I., Masters, C.L., Adlard, P.A., 2014a. The effect of paraformaldehyde fixation and sucrose cryoprotection on metal concentration in murine neurological tissue. Journal of Analytical Atomic Spectrometry.

Hare, D.J., Gerlach, M., Riederer, P., 2012b. Considerations for measuring iron in post-mortem tissue of Parkinson's disease patients. Journal of Neural Transmission 119, 1515-1521.

Hare, D.J., Lear, J., Bishop, D., Beavis, A., Doble, P.A., 2013b. Protocol for production of matrix-matched brain tissue standards for imaging by laser ablation-inductively coupled plasma-mass spectrometry. Analytical Methods 5, 1915-1921.

Hare, D.J., Lei, P., Ayton, S., Roberts, B.R., Grimm, R., George, J.L., Bishop, D.P., Beavis, A.D., Donovan, S.J., McColl, G., Volitakis, I., Masters, C.L., Adlard, P.A., Cherny, R.A., Bush, A.I., Finkelstein, D.I., Doble, P.A., 2014b. An iron–dopamine index predicts risk of parkinsonian neurodegeneration in the substantia nigra pars compacta. Chemical Science 5, 2160-2169.

Hare, D.J., New, E.J., de Jonge, M.D., McColl, G., 2015. Imaging metals in biology: balancing sensitivity, selectivity and spatial resolution. Chemical Society Reviews 44, 5941-5958.

James, S.A., Hare, D.J., Jenkins, N.L., de Jonge, M.D., Bush, A.I., McColl, G., 2016. φXANES: In vivo imaging of metal-protein coordination environments. Scientific Reports 6, 20350.

Langkammer, C., Krebs, N., Goessler, W., Scheurer, E., Ebner, F., Yen, K., Fazekas, F., Ropele, S., 2010. Quantitative MR Imaging of Brain Iron: A Postmortem Validation Study. Radiology 257, 455-462.

Langkammer, C., Krebs, N., Goessler, W., Scheurer, E., Yen, K., Fazekas, F., Ropele, S., 2012a. Susceptibility induced gray–white matter MRI contrast in the human brain. NeuroImage 59, 1413-1419.

Langkammer, C., Ropele, S., Pirpamer, L., Fazekas, F., Schmidt, R., 2014. MRI for iron mapping in Alzheimer's disease. Neurodegenerative Diseases 13, 189-191.

Langkammer, C., Schweser, F., Krebs, N., Deistung, A., Goessler, W., Scheurer, E., Sommer, K., Reishofer, G., Yen, K., Fazekas, F., Ropele, S., Reichenbach, J.R., 2012b. Quantitative susceptibility mapping (QSM) as a means to measure brain iron? A post mortem validation study. NeuroImage 62, 1593-1599.

Lear, J., Hare, D.J., Fryer, F., Adlard, P.A., Finkelstein, D.I., Doble, P.A., 2012. High-resolution elemental bioimaging of Ca, Mn, Fe, Co, Cu, and Zn employing LA-ICP-MS and hydrogen reaction gas. Analytical Chemistry 84, 6707-6714.

Leskovjan, A.C., Kretlow, A., Lanzirotti, A., Barrea, R., Vogt, S., Miller, L.M., 2011. Increased brain iron coincides with early plaque formation in a mouse model of Alzheimer's disease. NeuroImage 55, 32-38.

Lodygensky, G.A., Marques, J.P., Maddage, R., Perroud, E., Sizonenko, S.V., Hüppi, P.S., Gruetter, R., 2012. In vivo assessment of myelination by phase imaging at high magnetic field. NeuroImage 59, 1979-1987.

Lovell, M.A., Robertson, J.D., Teesdale, W.J., Campbell, J.L., Markesbery, W.R., 1998. Copper, iron and zinc in Alzheimer's disease senile plaques. Journal of the Neurological Sciences 158, 47-52.

Medina, D., deToledo-Morrell, L., Urresta, F., Gabrieli, J.D.E., Moseley, M., Fleischman, D., Bennett, D.A., Leurgans, S., Turner, D.A., Stebbins, G.T., 2006. White matter changes in mild cognitive impairment and AD: A diffusion tensor imaging study. Neurobiology of Aging 27, 663-672.

Miliszkiewicz, N., Walas, S., Tobiasz, A., 2015. Current approaches to calibration of LA-ICP-MS analysis. Journal of Analytical Atomic Spectrometry 30, 327-338.

Miyajima, H., Takahashi, Y., Kono, S., Sugimoto, M., Suzuki, Y., Hishida, A., Sakamoto, M., Oucm, Y., 2002. Glucose and Oxygen Hypometabolism in Aceruloplasminemia Brains. Internal Medicine 41, 186-190.

O'Reilly, J., Douglas, D., Braybrook, J., So, P.W., Vergucht, E., Garrevoet, J., Vekemans, B., Vincze, L., Goenaga-Infante, H., 2014. A novel calibration strategy for the quantitative imaging of iron in biological tissues by LA-ICP-MS using matrix-matched standards and internal standardisation. Journal of Analytical Atomic Spectrometry 29.

Olmos-Alonso, A., Schetters, S.T.T., Sri, S., Askew, K., Mancuso, R., Vargas-Caballero, M., Holscher, C., Perry, V.H., Gomez-Nicola, D., 2016. Pharmacological targeting of CSF1R inhibits microglial proliferation and prevents the progression of Alzheimer’s-like pathology. Brain DOI: 10.1093/brain/awv379.

Ong, W.-Y., Farooqui, A.A., 2005. Iron, neuroinflammation, and Alzheimer's disease. Journal of Alzheimer's Disease 8, 183-200.

Peters, D.G., Connor, J.R., Meadowcroft, M.D., 2015. The relationship between iron dyshomeostasis and amyloidogenesis in Alzheimer's disease: Two sides of the same coin. Neurobiology of Disease 81, 49-65.

Raven, E.P., Lu, P.H., Tishler, T.A., Heydari, P., Bartzokis, G., 2013. Increased iron levels and decreased tissue integrity in hippocampus of Alzheimer's disease detected in vivo with magnetic resonance imaging. Journal of Alzheimer's Disease 37, 127-136.

Rembach, A., Hare, D.J., Lind, M., Fowler, C.J., Cherny, R.A., McLean, C., Bush, A.I., Masters, C.L., Roberts, B.R., 2013. Decreased Copper in Alzheimer's Disease Brain Is Predominantly in the Soluble Extractable Fraction. International Journal of Alzheimer's Disease 2013, 1-7.

Riederer, P., Sofic, E., Rausch, W.-D., Schmidt, B., Reynolds, G.P., Jellinger, K., Youdim, M.B.H., 1989. Transition Metals, Ferritin, Glutathione, and Ascorbic Acid in Parkinsonian Brains. Journal of Neurochemistry 52, 515-520.

Rossi, M., Ruottinen, H., Soimakallio, S., Elovaara, I., Dastidar, P., 2013. Clinical MRI for iron detection in Parkinson's disease. Clinical Imaging 37, 631-636.

Schindelin, J., Arganda-Carreras, I., Frise, E., Kaynig, V., Longair, M., Pietzsch, T., Preibisch, S., Rueden, C., Saalfeld, S., Schmid, B., Tinevez, J.-Y., White, D.J., Hartenstein, V., Eliceiri, K., Tomancak, P., Cardona, A., 2012. Fiji: an open-source platform for biological-image analysis. Nature Methods 9, 676-682.

Schipper, H.M., 2004. Brain iron deposition and the free radical-mitochondrial theory of ageing. Ageing Research Reviews 3, 265-301.

Schrag, M., Dickson, A., Jiffry, A., Kirsch, D., Vinters, H.V., Kirsch, W., 2010. The effect of formalin fixation on the levels of brain transition metals in archived samples. BioMetals 23, 1123-1127.

Stüber, C., Morawski, M., Schäfer, A., Labadie, C., Wähnert, M., Leuze, C., Streicher, M., Barapatre, N., Reimann, K., Geyer, S., Spemann, D., Turner, R., 2014. Myelin and iron concentration in the human brain: A quantitative study of MRI contrast. NeuroImage 93, 95-106.

Thompson, P.M., Hayashi, K.M., de Zubicaray, G., Janke, A.L., Rose, S.E., Semple, J., Herman, D., Hong, M.S., Dittmer, S.S., Doddrell, D.M., Toga, A.W., 2003. Dynamics of gray matter loss in Alzheimer's disease. Journal of Neuroscience 23, 994-1005.

van Duijn, S., Nabuurs, R.J.A., van Duinen, S.G., Natte, R., 2013. Comparison of Histological Techniques to Visualize Iron in Paraffin-embedded Brain Tissue of Patients with Alzheimer's Disease. Journal of Histochemistry and Cytochemistry 61, 785-792.

Ward, R.R., Zucca, F.A., Duyn, J.H., Crichton, R.R., Zecca, L., 2014. The role of iron in brain ageing and neurodegenerativedisorders. Lancet Neurology 13, 1045-1060.

Wong, B.X., Tsatsanis, A., Lim, L.Q., Adlard, P.A., Bush, A.I., Duce, J.A., 2014. β-Amyloid Precursor Protein Does Not Possess Ferroxidase Activity but Does Stabilize the Cell Surface Ferrous Iron Exporter Ferroportin. PLoS One 9, e114174.

Yeatman, J.D., Wandell, B.A., Mezer, A.A., 2014. Lifespan maturation and degeneration of human brain white matter. Nature Communications 5, 4932.

Zeineh, M.M., Chen, Y., Kitzler, H.H., Hammond, R., Vogel, H., Rutt, B.K., 2015. Activated iron-containing microglia in the human hippocampus identified by

magnetic resonance imaging in Alzheimer disease. Neurobiology of Aging 36, 2483-2500.

Zhu, W.-Z., Zhong, W.-D., Wang, W., Zhan, C.-J., Wang, C.-Y., Qi, J.-P., Wang, J.-Z., Lei, T., 2009. Quantitative MR Phase-corrected Imaging to Investigate Increased Brain Iron Deposition of Patients with Alzheimer Disease. Radiology 253, 497-504.